Research on Chemical Intermediates (2022) 48:4729–4751
https://doi.org/10.1007/s11164-022-04831-5

One-pot synthesis, molecular docking, ADMET, and DFT studies of novel pyrazolines as promising SARS-CoV-2 main protease inhibitors

Rezan Huseen Hama Salih[1] · Aso Hameed Hasan[1,2] · Awaz Jamil Hussein[3] · Mohammed Kareem Samad[3] · Sonam Shakya[4] · Joazaizulfazli Jamalis[2] · Farouq Emam Hawaiz[3] · Mohammad Rizki Fadhil Pratama[5,6]

Received: 19 April 2022 / Accepted: 1 September 2022 / Published online: 13 September 2022

Abstract

Pyrazoline and its derivatives have numerous prominent pharmacological effects. Focusing on its anti-viral property, we have designed and synthesized three novel pyrazoline derivatives (**A1–A3**) through one-pot three components and characterized them using different spectroscopic techniques (FT-IR, ^{1}H NMR, ^{13}C NMR, and UV). These compounds were evaluated against SARS-CoV-2 main protease utilizing in-silico molecular docking studies. The docking results displayed good inhibitory activity of the synthesized compounds. Among them, compound **A2** was the most active against targeted protein. The drug-likeness and ADMET properties were predicted to have varied profiles but could still be developed, especially **A2**. DFT/TD-DFT calculations through B3LYP/6-311G++ level of theory were applied to provide comparable theoretical data along with MEP map and electronic energy gap of HOMO → LUMO.

Keywords Pyrazoline · One-pot synthesis · Molecular docking · ADMET · DFT

✉ Aso Hameed Hasan
aso.hameed@garmian.edu.krd

[1] Department of Chemistry, College of Science, University of Garmian, Kalar, Kurdistan Region-Iraq 46021, Iraq

[2] Department of Chemistry, Faculty of Science, University Teknologi Malaysia, 81310 Johor Bahru, Johor, Malaysia

[3] Department of Chemistry, College of Education, Salahaddin University, Erbil, Kurdistan Region-Iraq 44001, Iraq

[4] Department of Chemistry, Faculty of Science, Aligarh Muslim University, Aligarh 202002, India

[5] Doctoral Program of Pharmaceutical Sciences, Universitas Airlangga, Jl Dr Ir Soekarno Kampus C UNAIR Mulyorejo, Surabaya, East Java 60115, Indonesia

[6] Department of Pharmacy, Universitas Muhammadiyah Palangkaraya, Jl RTA Milono Km 1.5 Pahandut, Palangka Raya, Central Kalimantan 73111, Indonesia

Introduction

Humanity is now plagued by the coronavirus disease 2019 (Covid-19) pandemic, which is caused by coronavirus 2 that causes severe acute respiratory syndrome (SARS-CoV-2) [1]. Even though COVID-19 is a viral infection, it can also affect a patient's immune system. Therefore, secondary bacterial or fungal infections can take hold [2, 3]. Researchers worldwide have been attempting to investigate the potential treatment and discovery of effective therapeutic drug candidates for the management of COVID-19. Furthermore, some reports proposed potential inhibitory agents against COVID-19 targets. Currently, several molecules are being tested for their efficacy on COVID-19 disease, some of which have reached clinical trials, while others are still in the preclinical phase [1, 4, 5, 6, 7, 8, 9]. Pyrazoline is a five-membered heterocyclic having two adjacent nitrogen atoms within the ring [10, 11]. Nitrogen-containing heterocycles have a wide range of applications in medicine [12, 13, 14]. Therefore, the chemistry of pyrazoline compounds has attracted the attention of researchers due to their important biological activities such as anti-bacterial, anti-inflammatory, anti-cancer, anti-fungal, anti-oxidant, anti-depressant, anti-leishmanial, anti-convulsant, and anti-tumor properties [15, 16, 17, 18, 19, 20, 21, 22, 23], especially as anti-viral agent [24, 25, 26, 27].

Hence, we designed novel pyrazoline derivatives via one-pot three-component condensation reaction, as this became preferred protocol and was used extensively for synthesizing new heterocyclic compounds due to its simple set-up procedure, reduced reaction time, excellent yields and reduced pollutant production. Computationally (in silico) evaluated them as a potential agent against SARS-CoV-2 main protease (M^{pro}) with the help of molecular docking simulation. Moreover, the current study is going to investigate the different properties including drug-likeness and pharmacokinetics properties, structural characterization, spectroscopic, thermodynamic, and vibrational phenomena with stabilization energy of all the synthesized compounds. Based on the findings of this investigation, researchers will be able to discover an effective drug to treat COVID-19.

Experimental

Preparation of 1-(4-((4-chlorobenzyl)oxy)phenyl)ethan-1-one (3)

In 250-mL round bottom flask, a mixture of 4-hydroxyacetophenone (25 mmol), 4-chlorobenzylchloride (30 mmol) in the presence of catalytic anhydrous potassium carbonate (50 mmol) was refluxed for 6 h with stirring in absolute ethanol (50 mL). The reaction completion was monitored by changing the color, then poured into cold water. The obtained precipitate was filtered, washed with cold ethanol, dried in an oven, and recrystallized from ethanol to give compound **3**. White powder; m.p.: 91.3–92.7 °C; yield; 97.0%; FT-IR (KBr) (υ_{max}/cm^{-1}): 3008

(C–H sp^2), 2873 (C–H sp^3), 1668 (C=O), 1597 (C=C); UV $\lambda_{max} = 336$ nm; ^{1}H NMR (400 MHz, $CDCl_3$) (ppm): δ 2.57 (3H, s, CH_3), 5.09 (2H, s, OCH_2), 6.95 (2H, d, $J = 8.4$ Hz, Ar–H), 7.35 (4H, m, Ar–H), 7.90 (2H, d, $J = 8.4$ Hz, Ar–H); ^{13}C NMR (100 MHz, $CDCl_3$) (ppm): δ 196.70 (C=O), 162.30 (C-4), 134.60 (C-6), 134.00 (C-9), 130.70 (C-7 and C-7′), 130.60 (C-2 and C-2′), 128.80 (C-8 and C-8′), 128.7 (C-3), 114.50 (C-3 and C-3′), 69.30 (C-5), 26.30 (CH_3).

One pot synthesis of pyrazoline derivatives (A1-A3)

In a round bottom flask, a mixture of compound **3** (7 mmol), substituted benzaldehydes (7 mmol), and thiosemicarbazide (10 mmol) were dissolved in absolute ethanol (30 mL). To this mixture a catalytic amount of sodium hydroxide (12 mmol) was added and refluxed with stirring. The completion of reaction was monitored by thin layer chromatography (TLC) in hexane/ethyl acetate as a solvent system. The solution was cooled to room temperature, filtered the obtained solid, washed with cold ethanol, and dried. The pure target compounds (**A1–A3**) were obtained by recrystallization from toluene.

5-(3-(Benzyloxy)phenyl)-3-(4-((4-chlorobenzyl)oxy) phenyl)-4,5-dihydro-1*H*-pyrazole-1-carbothioamide (A1)

Pale yellow; m.p.: 210.3–211.8 °C; yield: 75.5%; $R_f = 0.36$ in *n*-Hex:EtOAc (1:1); FT-IR (KBr) (υ_{max}/cm^{-1}): 3487, 3360 (NH_2), 1604 (C=C), 1471 (C=N), 1355 (C=S); UV $\lambda_{max} = 360$ nm; ^{1}H NMR (400 MHz, $CDCl_3$) (ppm): δ 3.16 (1H, dd, $J = 4.0$ and 16.0 Hz, H_a-C_{11}), 3.78 (1H, dd, $J = 4.0$ and 16.0 Hz, H_b-C_{11}), 4.99 (2H, s, OCH_2), 5.09 (2H, s, OCH_2), 5.99 (1H, dd, $J = 4.0$ and 12.0 Hz, H-C_{12}), 6.16 (2H, s, NH_2), 6.82–7.77 (4H, m, Ar–H), 6.99 (2H, d, $J = 8.0$, H-7 and H-7′), 7.25–7.38 (16H, m, Ar–H), 7.65 (2H, d, $J = 8.0$ Hz, H-8 and H-8′); ^{13}C NMR (100 MHz, $CDCl_3$) (ppm): δ 176.37 (C-24), 160.73 (C-6), 158.94 (C-15), 155.68 (C-10), 143.58 (C-13), 135.37 (C-20), 134.77 (C-4), 133.69 (C-23), 130.04 (C-1), 129.02 (C-3 and C-3′), 128.93 (C-21 and C-21′), 128.86 (C-17), 128.74 (C-22 and C-22′), 128.69 (C-2 and C-2′), 128.21 (C-8 and C-8′), 123.55 (C-9), 118.23 (C-18), 115.16 (C-7 and C-7′), 113.60 (C-16), 112.17 (C-14), 69.32 (C-5), 69.20 (C-19), 63.24 (C-12), 43.07 (C-11).

5-(3-(Benzyloxy)phenyl)-3-(4-((4-chlorobenzyl)oxy) phenyl)-4,5-dihydro-1*H*-pyrazole-1-carbothioamide (A2)

White powder; m.p.: 203.7–205.4 °C; yield; 73.3%; $R_f = 0.43$ in *n*-Hex:EtOAc (1:1); FT-IR (KBr) (υ_{max}/cm^{-1}): 3423, 3236 (NH_2), 1591 (C=C), 1456 (C=N), 1382 (C=S); UV $\lambda_{max} = 362$ nm; ^{1}H NMR (400 MHz, $CDCl_3$) (ppm): δ 3.14 (1H, s, H_a-C_{11}), 3.77 (1H, s, H_b-C_{11}), 5.08 (4H, s, 2× OCH_2), 5.99 (1H, s, H_X-C_{12}), 6.84–7.65 (16H, m, Ar–H); ^{13}C NMR (100 MHz, $CDCl_3$) (ppm): δ 176.41 (C-24), 160.70 (C-6), 159.28 (C-15), 155.10 (C-10), 137.82 (C-13), 134.72 (C-20), 129.94 (C-4), 128.98 (C-23), 128.84 (C-1), 128.67 (C-3 and C-3′), 128.50 (C-21 and C-21′),

128.17 (C-17), 127.93 (C-22 and C-22′), 127.63 (C-2 and C-2′), 125.25 (C-8 and C-8′), 123.58 (C-9), 117.97 (C-18), 115.11 (C-7 and C-7′), 113.45 (C-16), 112.24 (C-14), 70.10 (C-5), 69.30 (C-19), 63.25 (C-12), 43.06 (C-11).

3-(4-((4-Chlorobenzyl)oxy)phenyl)-5-(3-((3-nitrobenzyl)oxy) phenyl)-4,5-dihydro-1*H*-pyrazole-1-carbothioamide (A3)

Pale brown; m.p.: 147.4–148.7 °C; yield: 64.6%; $R_f = 0.32$ in *n*-Hex:EtOAc (1:1); FT-IR (KBr) (υ_{max}/cm^{-1}): 3471, 3354 (NH_2), 1597 (C=C), 1471 (C=N), 1346 (C=S); UV $\lambda_{max} = 294$ nm; ^{1}H NMR (400 MHz, $CDCl_3$) (ppm): δ 3.15 (1H, d, $J = 16.0$ Hz, H_a-C_{11}), 3.72 (1H, dd, $J = 16.0$ Hz, H_b-C_{11}), 3.75 (1H, s, –CH-H_X-C_{12}), 5.07 (2H, s, –OCH_2), 5.08 (2H, s, –OCH_2), 6.38 (2H, s, NH_2), 5.99 (1H, d, $J = 12.0$ Hz, H-14), 6.85–7.73 (13H, m, Ar–H), 8.99 (1H, d, $J = 8.0$ Hz, H-23), 8.11 (1H, s, H-21); ^{13}C NMR (100 MHz, $CDCl_3$) (ppm): δ 179.27 (C-26), 160.74 (C-6), 158.56 (C-15), 155.73 (C-10), 148.29 (C-22), 143.83 (C-20), 139.08 (C-13), 134.82 (C-4), 133.95 (C-25), 133.32 (C-1), 130.20 (C-24), 129.54 (C-3 and C-3′), 129.05 (C-17), 128.23 (C-2 and C-2′), 125.31 (C-9), 123.47 (C-8 and C-8′), 122.83 (C-21), 118.53 (C-23), 115.15 (C7 and C-7′), 114.69 (C-18), 113.62 (C-16), 112.28 (C-14), 69.29 (C-5), 68.61 (C-19), 63.21 (C-12), 43.03 (C-11).

Molecular docking study

Ligand preparation

The 3D structures of titled compounds were drawn, and energy of each compound was minimized and saved in the pdb format by using Avogadro [28]. Subsequently, AutoDock Tools 4.2 [29] was used to open the pdb files, and torque adjustment was made by detecting roots and adjusting as desired. Then, the files were saved in the pdbqt format. Meantime, the structure data format (SDF) structure of the control, lopinavir (CID: 92727), was downloaded from the PubChem database (www.pubchem.ncbi.nlm.nih.gov). The structure data file (SDF) format was subjected to the energy minimization process using MMFF94 (Merck Molecular Force Field 94) force field algorithm [30], the minimized structure was converted into PDBQT format using PyRx before performing molecular docking analysis.

Protein preparation

The 3D crystal structure of SARS-CoV-2 (M^{pro}) was retrieved from the Protein Databank (http://www.rcsb.org) with PDB ID (6LU7). The co-crystallized ligand and water molecules were removed utilizing Discovery Studio Visualizer [31]. Afterward, polar hydrogens and Kollman charges were added. Partial charges of the

molecule were calculated using the Gasteiger method. The prepared file was saved as a pdbqt format for molecular docking using AutoDock Tools 4.2 [29].

Molecular docking

Molecular docking of the ligands was investigated by using the AutoDock Vina program [32]. Vina software was run in exhaustiveness = 8. The binding site was selected based on its co-crystallized ligand (N3) with the target protein [33]. Affinity scores (in kcal/mol) given by AutoDock Vina for all the compounds were obtained and ranked based on the free energy binding theory (more negative value means greater binding affinity). The resulting docking of ligand-receptor complexes with higher binding affinity was analyzed and drafted to 2D and 3D figures with the help of the DS Visualizer and UCSF Chimera.

ADMET analysis

According to the reported procedures, as described in the literature [34], prediction of drug-likeness and ADMET (Absorption, Distribution, Metabolism, Excretion, and Toxicity) properties of the synthesized compounds was carried out utilizing online servers such as SwissADME, ProTox-II, and pkCSM.

Density functional theory

In order to understand the spectral assignments, and to study the molecular geometry and electronic transitions of the synthesized compounds (**A1**, **A2**, and **A3**), a computational study was taken into account, to explore the molecular interactions in more detail. The Gaussian 09RevD.01 program [35] was used for theoretical studies. Gradient corrected correlation with Pople's basis set B3LYP/6-311G++ was applied. The gauge independent atomic orbital (GIAO) and Integral Equation Formalism Polarizable Continuum Model (IEFPCM) with the same functional set were used for computing ^{1}H-NMR chemical shifts in the liquid phase [36, 37, 38, 39, 40, 41, 42]. Optimized structure of **A1**, **A2**, and **A3** was also obtained using the B3LYP/6-311G++ basis set. Highest occupied molecular orbital (HOMO), lowest unoccupied molecular orbital (LUMO), and electrostatic potential map (MEP) were calculated. The calculated IR frequencies through this method are found to be positive, indicating that the optimized structure is at a minimum on the potential energy surface. In the FTIR spectrum, bands that appeared were assigned with full accuracy, using animated modes of vibrations. The frontier molecular orbitals help in determining the chemical stability of the system. Moreover, structure-based molecular properties like atomic charges, total energy, stabilization energy, electronic properties, bond lengths, frontier molecular orbitals, and molecular electrostatic potential were calculated by this theory in the gas phase. For visualization of obtained DFT results, ChemCraft 1.5 software [43] was used [43].

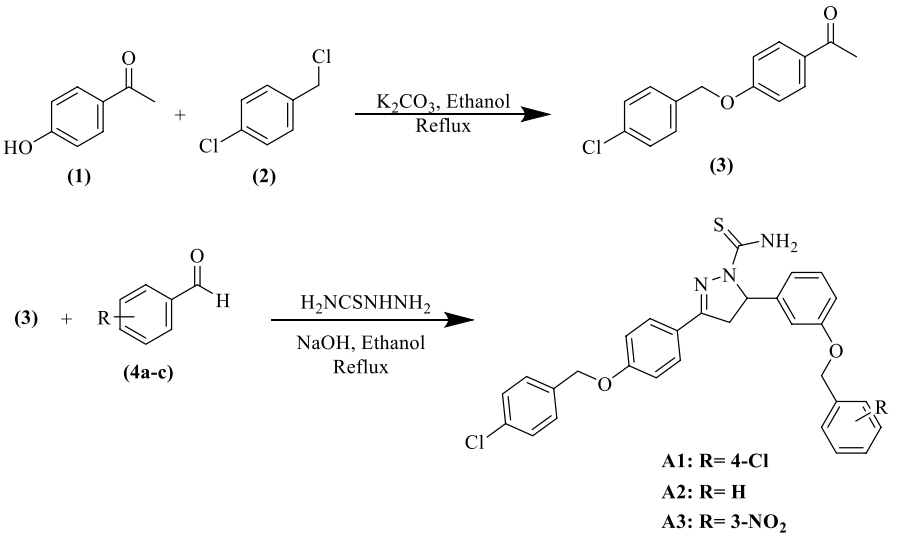

Scheme 1 synthesis of compounds (**A1**–**A3**)

Results and discussion

Chemistry

1-(4-((4-Chlorobenzyl)oxy)phenyl)ethan-1-one (**3**) was prepared in excellent yield (97%) based on of Williamson synthesis of ether by direct benzylation of *para*-hydroxy acetophenone with 4-chlorobenzylchloride, in the presence of anhydrous potassium carbonate in ethanol. The synthesis of pyrazoline derivatives (**A1–A3**) was accomplished via the condensation reaction of compound **3**, substituted benzaldehydes with thiosemicarbazide in dilute ethanolic sodium hydroxide solution (Scheme 1). The structures of synthesized pyrazolines **(A1–A3)** were confirmed by FT-IR, ^{1}H-NMR, ^{13}C-NMR, and UV–Vis spectroscopy. In FT-IR spectra of pyrazolines the disappearance of a band in the range of 1653–1645 cm^{-1} for carbonyl groups (C=O), were considered as good evidence to produce pyrazoline, all spectra exhibited a characteristic two bands at 3400–3200 cm^{-1} corresponding to the (NH_2) stretching of carbothioamide group attached to pyrazoline ring, also the appearance of the strong band at 1492–1456 cm^{-1} for C=N stretching vibration, which indicates the presence of pyrazoline ring, two bands at 1608–1597 cm^{-1} and 1382–1340 cm^{-1} referring to (C=C) and (C=S) double bond, respectively. The ^{1}H-NMR spectra of pyrazolines display doublet to doublet (dd) signals corresponding to three protons (two germinal and one vicinal) of C_{11} and C_{12} of pyrazoline ring; they form a characteristic ABX spin system explaining the inequivalence of protons at C_{11}.

Molecular docking study

Molecular docking was investigated by AutoDock Vina software due to its excellent speed and providing low root-mean-square deviation (RMSD) [32]. The binding affinity of titled compounds was compared with lopinavir which was used as a positive drug for comparison purposes which was recommended for clinical therapeutic [44]. The binding affinities of the synthesized compounds **A1** and **A2** (−8.2and −8.3 kcal/mol, respectively) were higher than the binding affinity of the positive drug lopinavir (−7.8 kcal/mol). Thus, these two compounds could be effectively inhibiting the SARS-CoV-2 main protease (M^{pro}). The compound **A3** has a slightly lower binding affinity (−7.5 kcal/mol) than the lopinavir. The docking results exhibited no significant differences in the binding affinities of compounds **A1** (with chloro substituent) and **A2** (without substituent), as shown in Table 1.

The A2-6LU7 complex established three hydrogen bonds with amino acid residues ASN238, LEU272, and LEU287. An alkyl interaction with LEU272 residue and π-alkyl interactions with TYR237 and LEU286 were also observed. Furthermore, it can form π-sigma interaction with LEU287. In contrast, compound **A1** showed additional hydrophobic and electrostatic interactions with ASP197 residue of target receptor via π-sigma and π-anion bonds. Moreover, compound **A3** (with nitro substituent) interacted with M^{pro}, formed five hydrogen bonds at residues THR199, ASN238, LEU271, ALA285, and LEU287. An alkyl and π-alkyl hydrophobic interactions were observed between this compound and the receptor. Additionally, amino acid residues ASP107 and LYS137 are involved in forming π-anion and π-cation electrostatic interactions, respectively. The docking interactions of synthesized compounds with the active site amino acid residues of SARS-CoV-2 (M^{pro}) are depicted in Fig. 1. The docking scores interaction modes of all docked ligands into the active site and the amino acid residues of M^{pro} are presented in Table 1.

Drug-likeness and ADMET prediction

The pharmacokinetic properties and toxicity profile of the pyrazolines (**A1–A3**) were predicted in-silico, as presented in Table 2. The obtained results are in agreement with parameters reported in the literature [45], as well as referring to Lipinski's rule of five (LRO5) [46]. The first parameter observed was molecular weight (Mol. Wt.), where all compounds met the LRO5 criteria, which were ≤500 g/mol. However, the Mol. Wt. of all ligands still met the criteria set by Chander et al. [45]. Then, all compounds showed a TPA value of less than 140 A^2, thus fulfilling the criteria in LRO5 [46], even though the compound **A3** showed a value that was close to the threshold. The number of hydrogen donor and acceptor groups of all compounds meets the LRO5 criteria, with no more than 5 and 10 groups, respectively. All compounds did not meet the criteria for Log *P* based on LRO5 [46], especially compound **A1**, whose Log *P* values were huge (>7.5). The high Log *P* value can affect the absorption and distribution of the compound, so it is necessary to consider ways to handle it [47]. Only compound **A3** showed

Table 1 Molecular docking scores and interaction modes between compounds and SARS-CoV-2 (PDB ID: 6LU7)

Ligand	Kcal/mol	Interaction					
		H-bond	Hydrophobic			Electrostatic	
			Alkyl	π-alkyl	π-sigma	π-anion	π-cation
A2	−8.3	ASN238, LEU272, LEU287	LEU272	TYR237, LEU286	LEU287		
A1	−8.2	ASN238, LEU272, LEU287	LEU272	TYR237, LEU286	ASP197, LEU287	ASP197	
A3	−7.5	THR199, ASN238, LEU271, ALA285, LEU287	LEU286	LEU286		ASP197	LYS137
Lopinavir	−7.8						

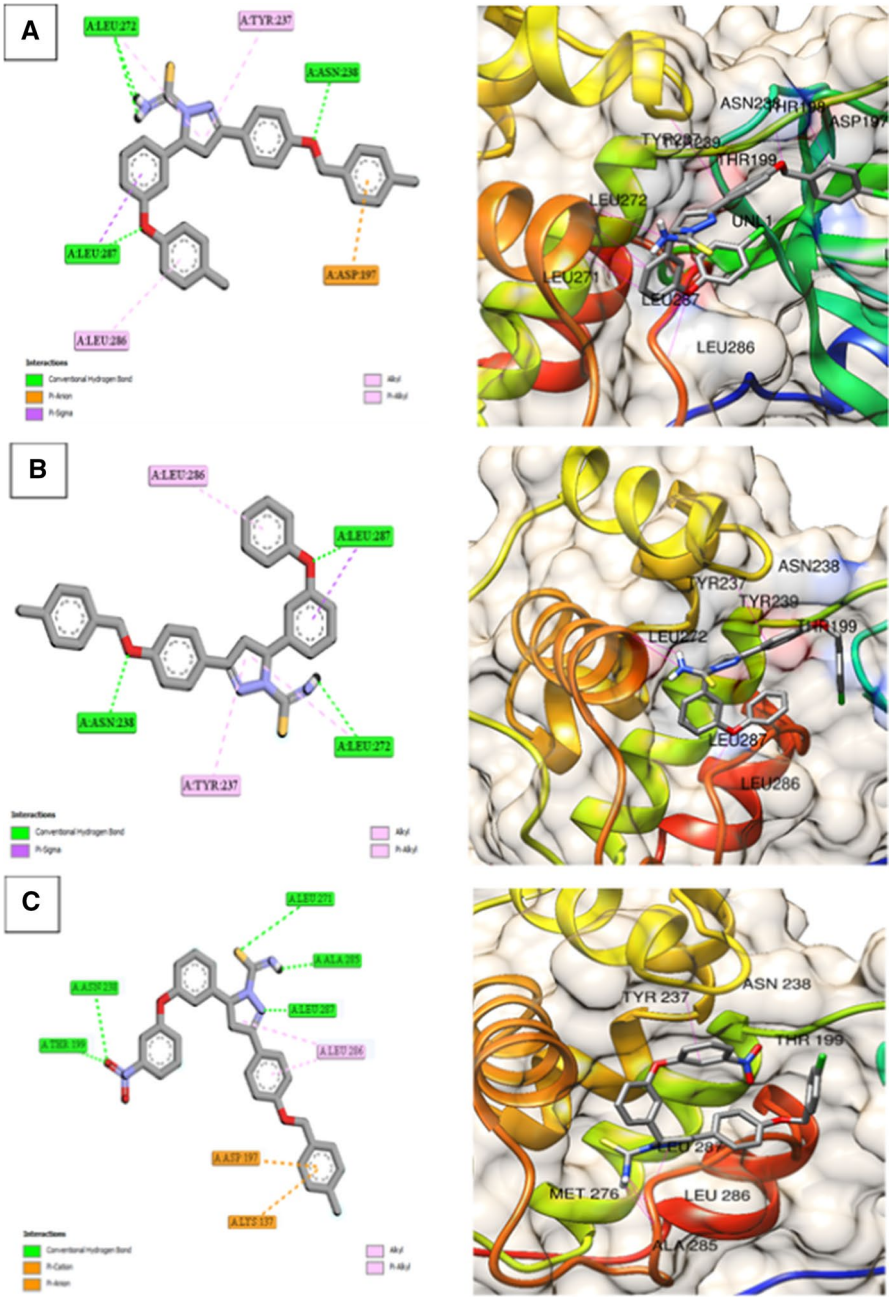

Fig. 1 Three-dimensional and two-dimensional diagrams illustrating the various interaction modes of (**A**) **A1**, (**B**) **A2**, and (**C**) **A3** within active site of SARS-CoV-2 (6LU7)

Table 2 ADMET properties of synthesized compounds

Compounds	A1	A2	A3
Molecular weight (g/mol)	528.077	562.522	573.074
Topological polar surface area (Å^2)	92.17	92.17	137.99
Hydrogen bond donor	1	1	1
Hydrogen bond acceptor	8	8	9
Aqueous solubility(log [mol/L])	−6.613	−6.621	−5.956
Predicted apparent Caco-2 cell permeability (10^{-6} cm/s)	1.021	1.008	0.604
Acute toxicity	IV	IV	IV
Predicted LD_{50} (mg/kg)	1000	1000	1000
Ames	NO	NO	YES

optimal Log *S* values, although all of them had good $CaCO_2$. The compound **A3** again is the only one that shows a relatively low Log *BB* value outside the optimal range, and also shows the highest amount of Rot, even though it is still in the optimal range.

Finally, all compounds are predicted to have moderate toxicity (harmful if swallowed) with an LD_{50} of 1000 mg/kg and are in class IV of the globally harmonized system of classification of labeling of chemicals [48]. However, compound **A3** was predicted to be a mutagen with a positive Ames test result. Further analysis of the target toxicity of each compound with ProTox-II is presented in Fig. 2. Among synthesized compounds, only **A3** showed the probability of toxicity to several targets such as carcinogenicity (carcino) and mutagenicity (mutagen), although with a low probability (< 0.7) [48]. Overall, compound **A1** shows absorption and distribution deficiencies, while **A3** compounds tend to be more toxic. Thus, compound **A2** has the most ideal ADMET properties compared to the two.

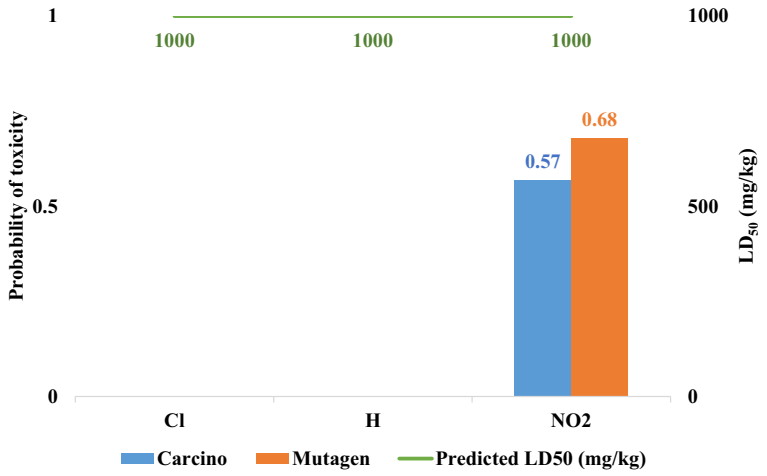

Fig. 2 Prediction of toxicity parameters with ProTox-II

DFT studies

The total SCF energy of the synthesized compounds **A1**, **A2**, and **A3** after 8, 16, and 40 optimization steps was obtained to be −2791.37, −2331.77, and −2387.12 a.u, respectively. The stabilization energy for **A1**, **A2**, and **A3** was calculated to be -288.81×10^3, −407.88, and -351.40×10^2 kcal/mol, respectively, which endorsed the stability of the compounds. The optimization of all compounds (**A1**, **A2**, and **A3**) was carried out through the B3LYP/6-311G++ calculations. Figure 3 shows the optimized structures of **A1**, **A2**, and **A3** having ground state minimum energy, strain-free lattice constants, and atomic coordinates. From the optimized structures, the bond lengths were also obtained, which are represented in Fig. 4 and Table 3. The obtained Mulliken charges of the titled compounds were compared, which showed the shift in Mulliken charges, indicating the compound formation has different structural values. Figure 3 and Table 4 represent the Mulliken atomic numbers scheme and atomic charges, respectively.

The molecular electrostatic potential (MEP) map (Fig. 5) represents the electrostatic potentials strength of reactants and synthesized moieties. The red color represents the electronegative area, and the blue color is for the electropositive

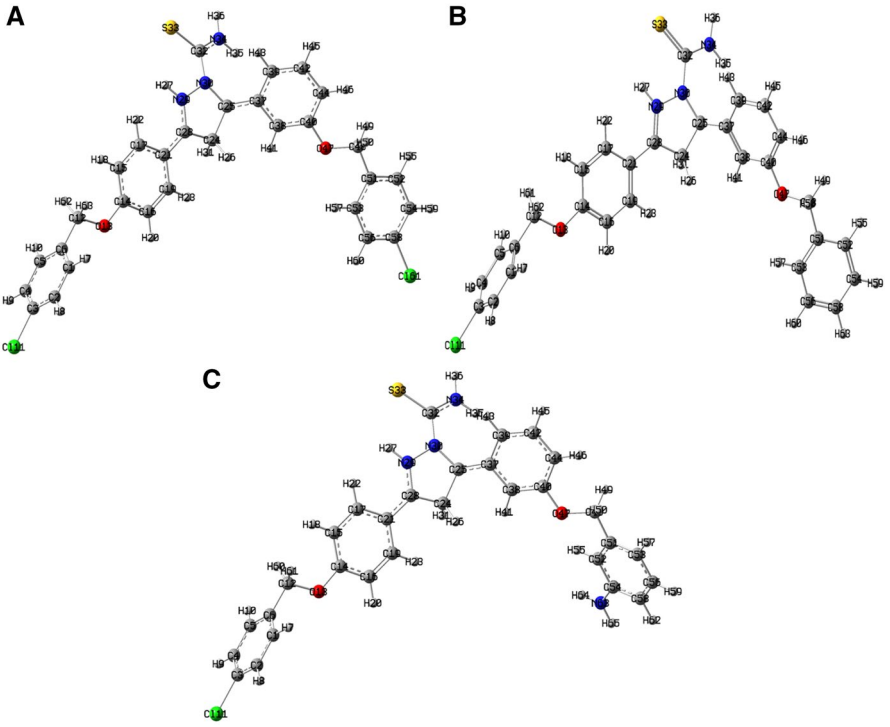

Fig. 3 Optimized structure of compounds (**a**) **A1**, (**b**) **A2**, and (**c**) **A3** with Mulliken atom numbering scheme

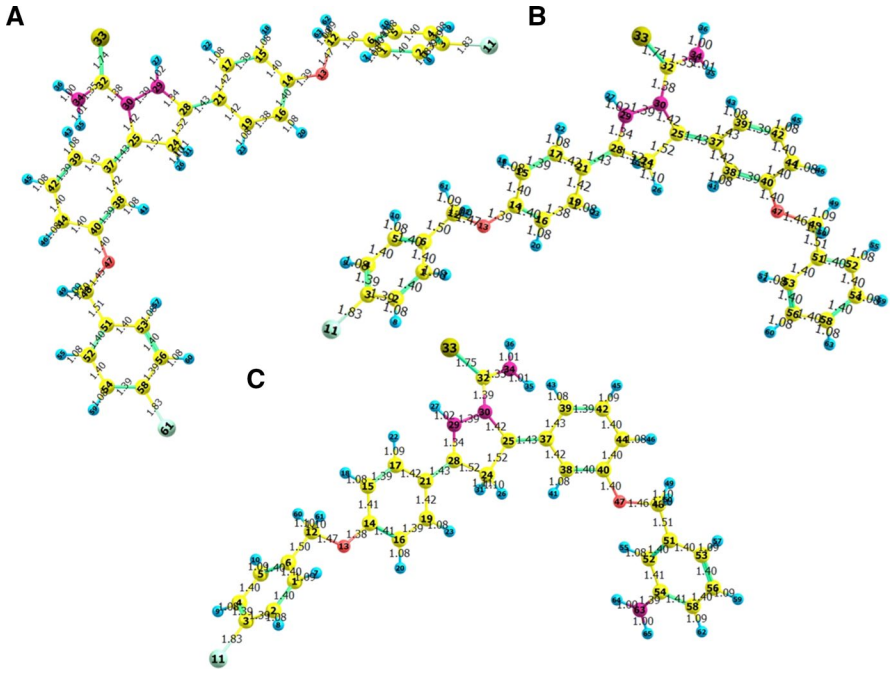

Fig. 4 Optimized structure of compounds (**a**) **A1**, (**b**) **A2**, and (**c**) **A3**, showing bond lengths

region. The interaction between the reactants can be studied by MEP, as the electron-deficient region lies at C and H of reactant and electron-rich at O atom. These results show the preferential binding sites over the molecule for the electrophilic and nucleophilic attacks [49, 50]. MEP map of the designed compounds is plotted from deep red to deep blue color scale as -5.159 e^{-2} to $+5.159$ e^{-2}, -4.970 e^{-2} to $+4.970$ e^{-2}, and -5.148 e^{-2} to $+5.148$ e^{-2} for **A1**, **A2**, and **A3**, respectively, as shown in Fig. 5. B3LYP/6-311G++ basis set was also used to investigate the IR spectrum theoretically. The comparison of experimental FTIR spectra of the synthesized compounds with the simulated spectra for **A1**, **A2**, and **A3** scaled at 0.9785, 0.9200, and 0.9190, respectively, are shown in Figs. 6, 7 and 8. The computed IR spectrum in animated modes was found to be compatible with few significant experimental vibrational signals in the FTIR spectra of the compounds [51]. The slight difference between theoretical and experimental frequencies is due to theoretical values being acquired in gas phase and experimental values being obtained in solid phase and also due to neglecting the incompleteness and anharmonicity of the basis set. Therefore, to reduce the differences, the scaling factor is used. The nature of the electronic transitions has been explored in the gas phase through TD-DFT method as shown in Fig. 9. Two absorption bands at 375 and 450 nm can be seen through TD-DFT calculations for **A1**. The simulated absorption bands at 450 and 375 nm are assigned to HOMO to LUMO and HOMO to LUMO + 1. Similar results were obtained for **A2** and **A3** from TD-DFT calculations.

Table 3 The bond lengths of the synthesized compounds obtained through DFT

S. no.	Atoms/bond length (Å)					
	A1		**A2**		**A3**	
1	R(1–2)	1.396	R(1–2)	1.396	R(1–2)	1.398
2	R(1–6)	1.401	R(1–6)	1.401	R(1–6)	1.404
3	R(1–7)	1.082	R(1–7)	1.082	R(1–7)	1.086
4	R(2–3)	1.39	R(2–3)	1.390	R(2–3)	1.394
5	R(2–8)	1.079	R(2–8)	1.079	R(2–8)	1.083
6	R(3–4)	1.39	R(3–4)	1.390	R(3–4)	1.393
7	R(3–11)	1.828	R(3–11)	1.829	R(3–11)	1.826
8	R(4–5)	1.396	R(4–5)	1.396	R(4–5)	1.399
9	R(4–9)	1.079	R(4–9)	1.079	R(4–9)	1.083
10	R(5–6)	1.401	R(5–6)	1.401	R(5–6)	1.403
11	R(5–10)	1.082	R(5–10)	1.082	R(5–10)	1.086
12	R(6–12)	1.501	R(6–12)	1.501	R(6–12)	1.502
13	R(12–13)	1.474	R(12–13)	1.474	R(12–13)	1.472
14	R(12–62)	1.092	R(12–61)	1.092	R(12–60)	1.096
15	R(12–63)	1.092	R(12–62)	1.092	R(12–61)	1.097
16	R(13–14)	1.386	R(13–14)	1.387	R(13–14)	1.385
17	R(14–15)	1.405	R(14–15)	1.405	R(14–15)	1.407
18	R(14–16)	1.403	R(14–16)	1.403	R(14–16)	1.406
19	R(15–17)	1.389	R(15–17)	1.389	R(15–17)	1.391
20	R(15–18)	1.079	R(15–18)	1.079	R(15–18)	1.083
21	R(16–19)	1.384	R(16–19)	1.384	R(16–19)	1.386
22	R(16–20)	1.08	R(16–20)	1.080	R(16–20)	1.083
23	R(17–21)	1.417	R(17–21)	1.417	R(17–21)	1.419
24	R(17–22)	1.082	R(17–22)	1.082	R(17–22)	1.086
25	R(19–21)	1.421	R(19–21)	1.421	R(19–21)	1.423
26	R(19–23)	1.08	R(19–23)	1.080	R(19–23)	1.084
27	R(21–28)	1.432	R(21–28)	1.431	R(21–28)	1.431
28	R(24–25)	1.525	R(24–25)	1.525	R(24–25)	1.524
29	R(24–26)	1.099	R(24–26)	1.099	R(24–26)	1.103
30	R(24–28)	1.522	R(24–28)	1.522	R(24–28)	1.522
31	R(24–31)	1.105	R(24–31)	1.105	R(24–31)	1.112
32	R(25–30)	1.421	R(25–30)	1.421	R(25–30)	1.417
33	R(25–37)	1.426	R(25–37)	1.427	R(25–37)	1.426
34	R(27–29)	1.017	R(27–29)	1.016	R(27–29)	1.020
35	R(28–29)	1.338	R(28–29)	1.339	R(28–29)	1.342
36	R(29–30)	1.391	R(29–30)	1.390	R(29–30)	1.390
37	R(30–32)	1.384	R(30–32)	1.384	R(30–32)	1.385
38	R(32–33)	1.745	R(32–33)	1.745	R(32–33)	1.749
39	R(32–34)	1.347	R(32–34)	1.347	R(32–34)	1.349
40	R(34–35)	1.008	R(34–35)	1.008	R(34–35)	1.011
41	R(34–36)	1.003	R(34–36)	1.003	R(34–36)	1.007
42	R(37–38)	1.422	R(37–38)	1.422	R(37–38)	1.423

Table 3 (continued)

S. no.	Atoms/bond length (Å)					
	A1		**A2**		**A3**	
43	R(37–39)	1.432	R(37–39)	1.431	R(37–39)	1.433
44	R(38–40)	1.392	R(38–40)	1.393	R(38–40)	1.395
45	R(38–41)	1.08	R(38–41)	1.080	R(38–41)	1.083
46	R(39–42)	1.387	R(39–42)	1.387	R(39–42)	1.390
47	R(39–43)	1.08	R(39–43)	1.080	R(39–43)	1.083
48	R(40–44)	1.4	R(40–44)	1.400	R(40–44)	1.403
49	R(40–47)	1.405	R(40–47)	1.402	R(40–47)	1.397
50	R(42–44)	1.404	R(42–44)	1.404	R(42–44)	1.405
51	R(42–45)	1.083	R(42–45)	1.083	R(42–45)	1.087
52	R(44–46)	1.079	R(44–46)	1.079	R(44–46)	1.082
53	R(47–48)	1.454	R(47–48)	1.456	R(47–48)	1.456
54	R(48–49)	1.094	R(48–49)	1.094	R(48–49)	1.101
55	R(48–50)	1.096	R(48–50)	1.096	R(48–50)	1.098
56	R(48–51)	1.508	R(48–51)	1.508	R(48–51)	1.510
57	R(51–52)	1.401	R(51–52)	1.401	R(51–52)	1.397
58	R(51–53)	1.401	R(51–53)	1.401	R(51–53)	1.405
59	R(52–54)	1.398	R(52–54)	1.397	R(52–54)	1.410
60	R(52–55)	1.083	R(52–55)	1.084	R(52–55)	1.084
61	R(53–56)	1.397	R(53–56)	1.396	R(53–56)	1.399
62	R(53–57)	1.079	R(53–57)	1.080	R(53–57)	1.086
63	R(54–58)	1.388	R(54–58)	1.397	R(54–58)	1.411
64	R(54–59)	1.079	R(54–59)	1.082	R(54–63)	1.386
65	R(56–58)	1.39	R(56–58)	1.398	R(56–58)	1.395
66	R(56–60)	1.08	R(56–60)	1.082	R(56–59)	1.086
67	R(58–61)	1.834	R(58–63)	1.082	R(58–62)	1.087
68					R(63–64)	1.005
69					R(63–65)	1.005

The ^{1}H-NMR spectra for all the compounds were also obtained through GIAO calculation, as shown in Figs. 10, 11 and 12 [51]. Frontier molecular orbitals (FMOs) are significant factors for explaining chemical behavior; hence, they were also computed theoretically. LUMO are generally electron acceptors, while HOMO are electron donors. The chemical stability of molecules is related to the energy gap between the HOMO and LUMO. According to the literature, compounds with a small energy gap have low kinetic stability, more chemical reactivity, and are soft in nature, whereas compounds with a large energy gap have high kinetic stability, less chemical reactivity, and are hard in nature [52]. Figure 13 represents the spatial arrangements of HOMO and LUMO along with their gap and associated energies. The HOMO–LUMO gap (ΔE) for compounds **A1**, **A2**, and **A3** were calculated to be 3.216, 3.156, and 2.622 eV, respectively [53]. On the basis of ΔE, the chemical reactivity of the compounds is arranged in the following sequence—**A1 > A2 > A3**.

Table 4 Mulliken atomic charges on the atoms of the optimized structure of the titled compounds

A1			A2			A3		
Mulliken atomic numbers/ Mulliken atomic charges								
1	C	−0.09663	1	C	−0.09799	1	C	−0.0889
2	C	−0.05658	2	C	−0.05673	2	C	−0.05779
3	C	−0.28835	3	C	−0.28837	3	C	−0.28679
4	C	−0.05667	4	C	−0.05665	4	C	−0.05844
5	C	−0.09767	5	C	−0.09638	5	C	−0.10434
6	C	0.0289	6	C	0.02878	6	C	0.02876
7	H	0.16969	7	H	0.16965	7	H	0.16993
8	H	0.19152	8	H	0.19128	8	H	0.19084
9	H	0.1915	9	H	0.19122	9	H	0.19036
10	H	0.1695	10	H	0.16945	10	H	0.16975
11	Cl	−0.01301	11	Cl	−0.01384	11	Cl	−0.01308
12	C	−0.24677	12	C	−0.24594	12	C	−0.24858
13	O	−0.5044	13	O	−0.5051	13	O	−0.50338
14	C	0.2788	14	C	0.27778	14	C	0.27679
15	C	−0.19588	15	C	−0.19584	15	C	−0.19768
16	C	−0.19079	16	C	−0.19078	16	C	−0.18968
17	C	−0.05001	17	C	−0.05052	17	C	−0.04908
18	H	0.18117	18	H	0.18037	18	H	0.18005
19	C	−0.08283	19	C	−0.08414	19	C	−0.08639
20	H	0.18216	20	H	0.18129	20	H	0.18032
21	C	−0.04972	21	C	−0.04866	21	C	−0.04486
22	H	0.16939	22	H	0.16865	22	H	0.1684
23	H	0.18185	23	H	0.18177	23	H	0.18121
24	C	−0.63412	24	C	−0.63298	24	C	−0.61926
25	C	0.31144	25	C	0.31268	25	C	0.32061
26	H	0.21514	26	H	0.21506	26	H	0.21667
27	H	0.39089	27	H	0.39072	27	H	0.39142
28	C	0.36127	28	C	0.3591	28	C	0.34802
29	N	−0.49401	29	N	−0.49453	29	N	−0.4963
30	N	−0.4569	30	N	−0.45762	30	N	−0.46603
31	H	0.20027	31	H	0.1993	31	H	0.19416
32	C	0.19441	32	C	0.19545	32	C	0.19612
33	S	−0.15294	33	S	−0.1548	33	S	−0.15819
34	N	−0.72191	34	N	−0.72185	34	N	−0.72204
35	H	0.37171	35	H	0.37201	35	H	0.37329
36	H	0.37122	36	H	0.3708	36	H	0.37094
37	C	−0.04855	37	C	−0.05053	37	C	−0.04191
38	C	−0.19693	38	C	−0.1974	38	C	−0.20431
39	C	−0.15232	39	C	−0.1517	39	C	−0.16724
40	C	0.24021	40	C	0.24059	40	C	0.24655
41	H	0.1626	41	H	0.16281	41	H	0.16176

Table 4 (continued)

A1			A2			A3		
42	C	−0.17033	42	C	−0.16989	42	C	−0.16767
43	H	0.16767	43	H	0.16675	43	H	0.16971
44	C	−0.15496	44	C	−0.15443	44	C	−0.15443
45	H	0.13791	45	H	0.13684	45	H	0.13723
46	H	0.16058	46	H	0.16115	46	H	0.16317
47	O	−0.54455	47	O	−0.54076	47	O	−0.5406
48	C	−0.19786	48	C	−0.20394	48	C	−0.20974
49	H	0.19108	49	H	0.18838	49	H	0.19336
50	H	0.19813	50	H	0.19501	50	H	0.19004
51	C	−0.02008	51	C	−0.0281	51	C	−0.04321
52	C	−0.13155	52	C	−0.13424	52	C	−0.11143
53	C	−0.06533	53	C	−0.06866	53	C	−0.14244
54	C	−0.06341	54	C	−0.16664	54	C	0.38504
55	H	0.16212	55	H	0.15141	55	H	0.17448
56	C	−0.06831	56	C	−0.17095	56	C	−0.17203
57	H	0.18345	57	H	0.17343	57	H	0.144
58	C	−0.28278	58	C	−0.12805	58	C	−0.16654
59	H	0.18419	59	H	0.14709	59	H	0.1371
60	H	0.18397	60	H	0.14698	60	H	0.19137
61	Cl	−0.03085	61	H	0.19162	61	H	0.19202
62	H	0.19215	62	H	0.19175	62	H	0.14512
63	H	0.1921	63	H	0.14883	63	N	−0.90598
						64	H	0.32101
						65	H	0.31876

Certain molecular properties in the gas phase related to chemical reactivity for the compounds are shown in Table 5 based on the optimized structure and HOMO–LUMO.

Conclusion

We have successfully synthesized three new pyrazoline analogues and evaluated their in silico inhibitory activity against SARS-CoV-2 M^{pro}. The results exhibited that all of them have potential inhibitory. Compound **A2** (−8.3 kcal/mol) was found to be the most potent SARS-CoV-2 M^{pro} inhibitor among the docked compounds. Furthermore, compound **A2** also showed more ideal ADMET properties compared to the other designed compounds. The optimized structures alone with the molecular properties were obtained for the synthesized compounds through theoretical DFT calculations, which supports the experimental

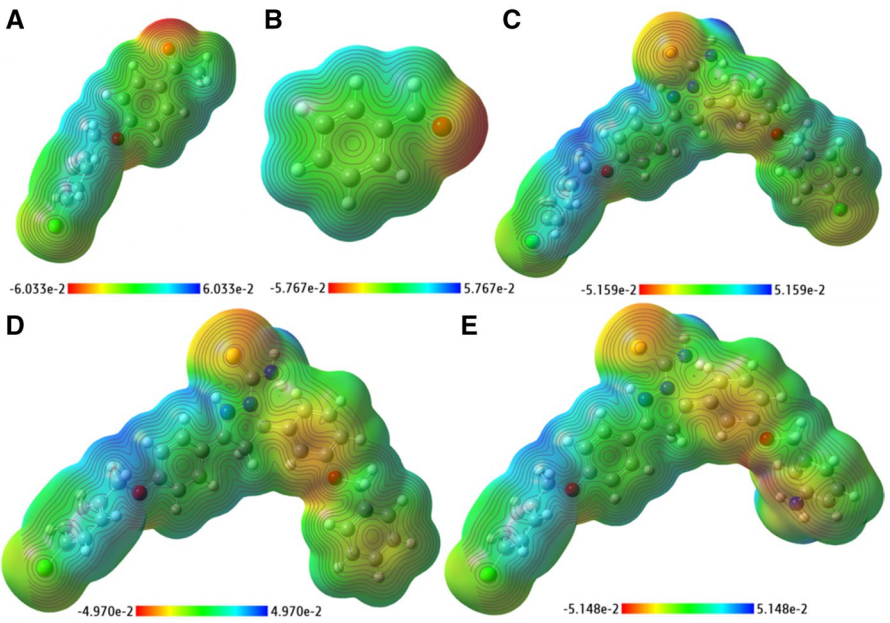

Fig. 5 MEP surface map of (**a**), reactant-**a** (**b**), reactant-**b** (**c**) **A1**, (**d**) **A2**, and (**e**) **A3** with respective color scales

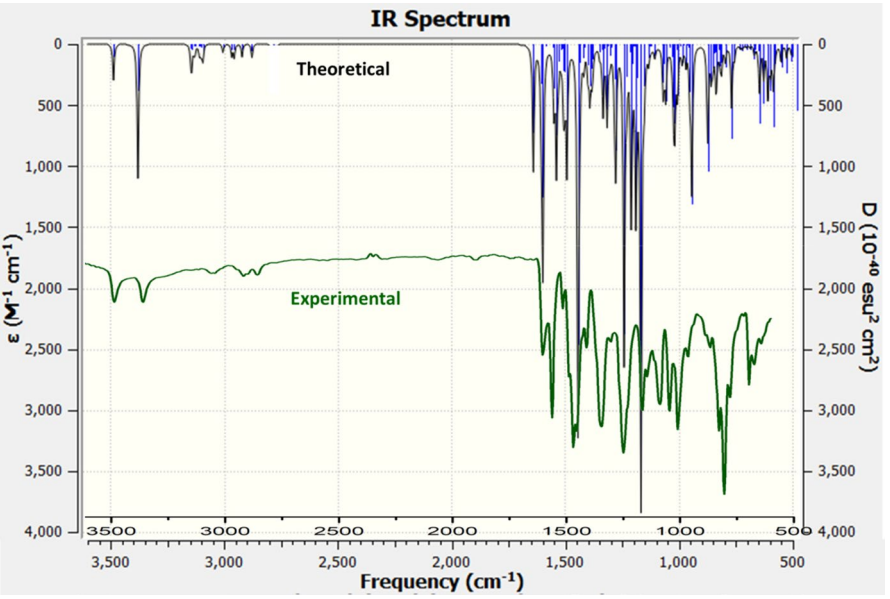

Fig. 6 FTIR spectra of **A1**, experimental (green) and computational (black)

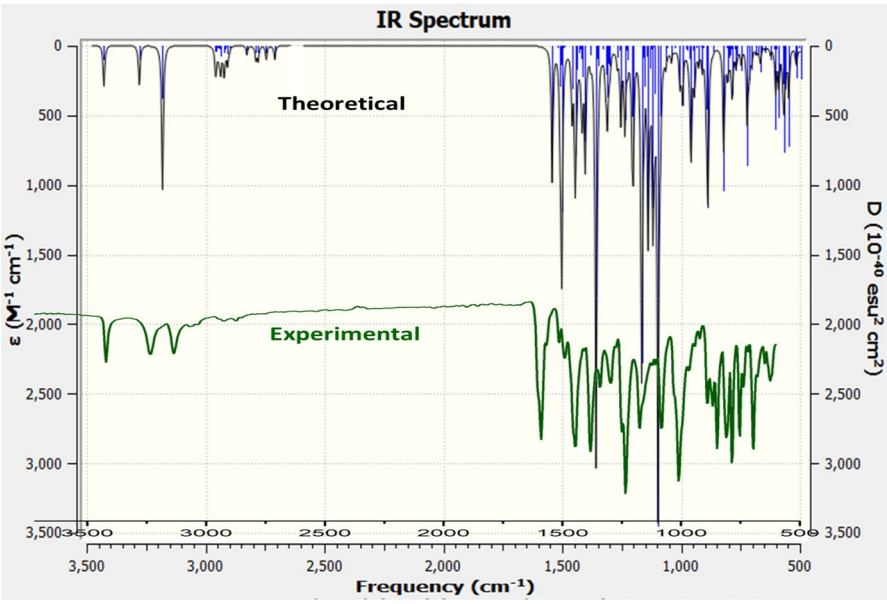

Fig. 7 FTIR spectra of **A2**, experimental (green) and computational (black)

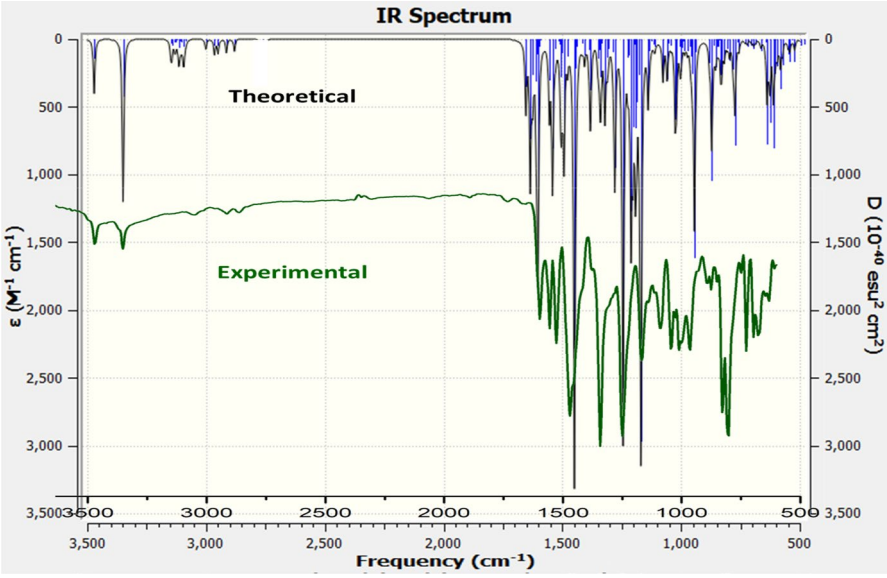

Fig. 8 FTIR spectra of **A3**, experimental (green) and computational (black)

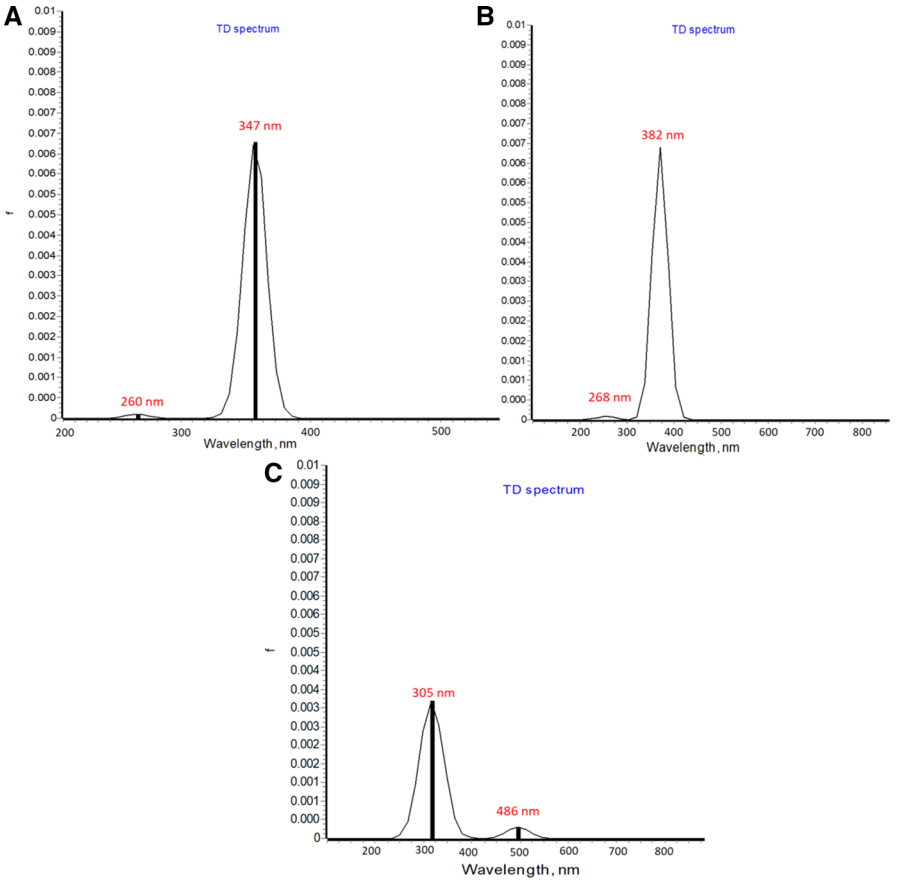

Fig. 9 UV–visible spectra of (**a**) **A1**, (**b**) **A2**, and (**c**) **A3** obtained through TD-DFT calculations

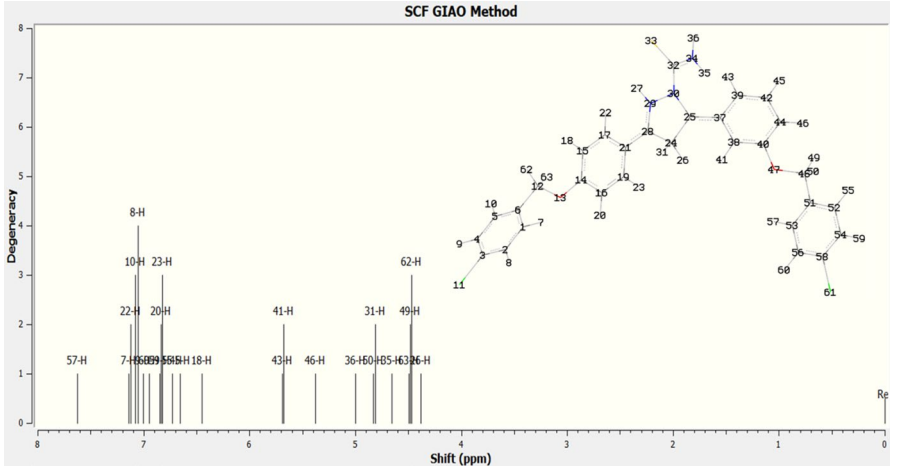

Fig. 10. ^{1}H NMR spectrum for **A1** calculated through DFT (GIAO) calculations

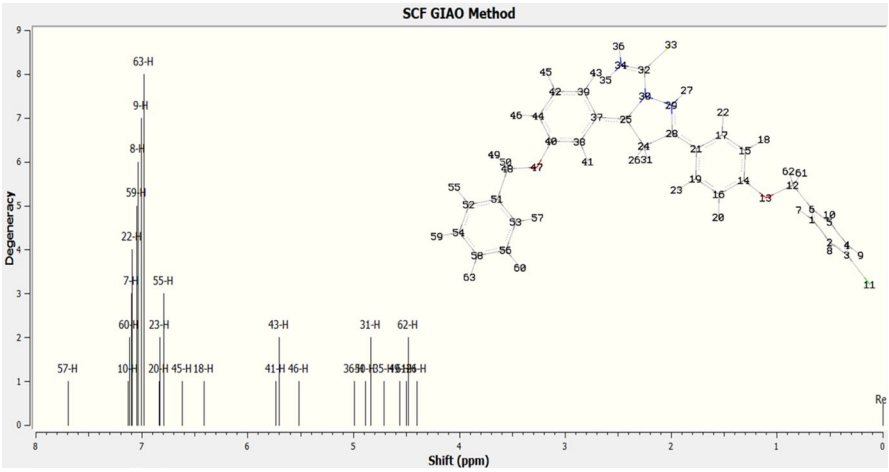

Fig. 11. ^{1}H NMR spectrum of **A2** calculated through DFT (GIAO) calculations

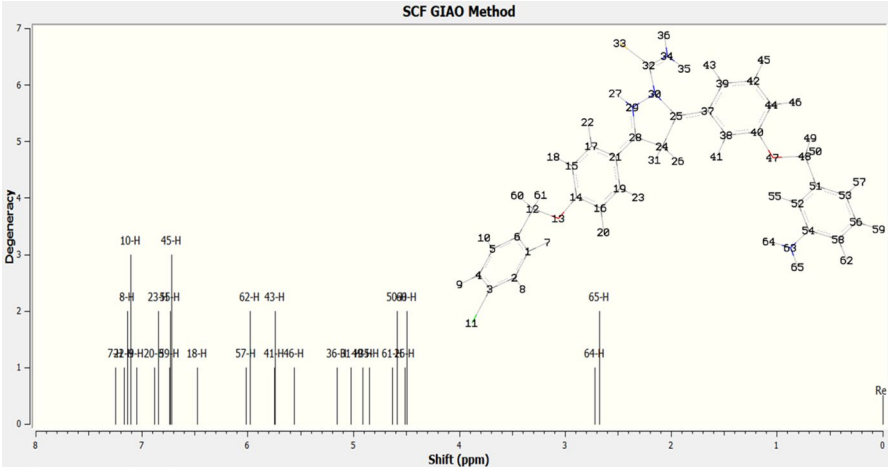

Fig. 12. ^{1}H NMR spectrum of **A3** calculated through DFT (GIAO) calculations

data. Various other theoretical molecular parameters calculated through DFT and in vitro evaluation against SARS-CoV-2 M^{pro} will help researchers for future investigations.

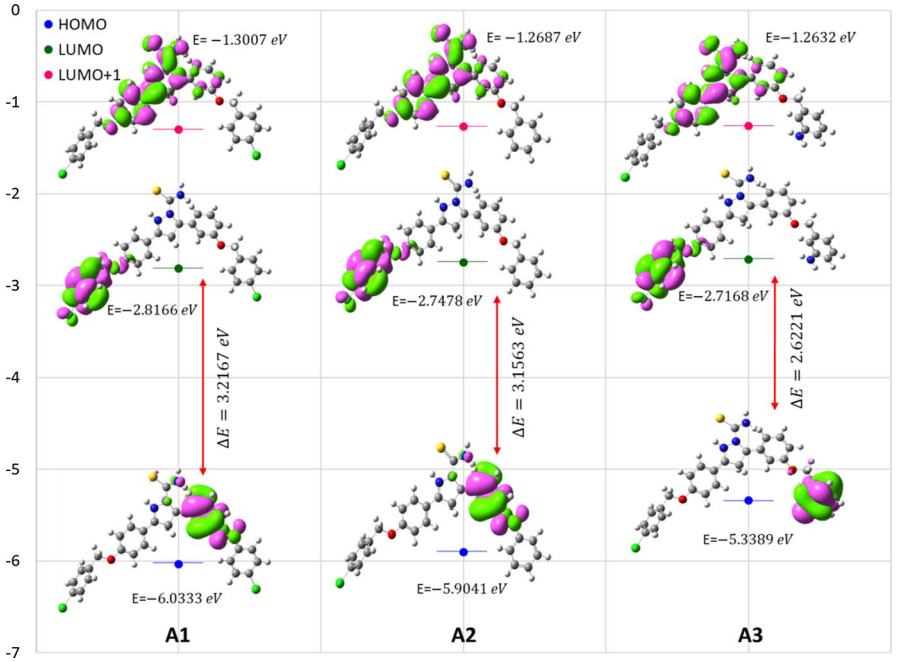

Fig. 13 Spatial plot of HOMO and LUMO with their energy gap

Table 5 Various other theoretical molecular parameters of the compounds and their constituents

Parameters	RB3LYP/6-311G++		
	A1	**A2**	**A3**
Minimum SCF energy (a.u.)	−2791.25089341	−2331.79962255	−2386.73822668
Stabilization energy (kcal/mol)	-288.81×10^{3}	−407.88	-351.40×10^{2}
Polarizability (α) (a.u.)	559.311624	546.570683	535.285008
Dipole moment (debye)	3.907789	2.630545	3.317812
Zero point vibrational energy (kcal/mol)	305.38410	311.69885	324.56856
Total thermal energy (kcal/mol)	326.740	332.206	345.938
Electronic spatial extent (a.u.)	62,027.6922	46,602.7123	49,737.2080
Frontier MO energies (eV)			
LUMO + 1	−1.3007	−1.2687	−1.2632
LUMO	−2.8166	−2.7478	−2.7168
HOMO	−6.0333	−5.9041	−5.3389
Gap (LUMO–HOMO)	3.2167	3.1563	2.6221

Supplementary Information The online version contains supplementary material available at https://doi.org/10.1007/s11164-022-04831-5.

Acknowledgements The authors wish to thank Universiti Teknologi Malaysia and the Ministry of Higher Education (MOHE) Malaysia for funding this research under the Fundamental Research Grant Scheme (FRGS/1/2019/STG01/UTM/02/7).

Declarations

Conflict of interest The authors have no conflict of interest to declare.

References

1. J. Dowarah, B.N. Marak, U.C.S. Yadav, V.P. Singh, Bioorg. Chem. **114**, 105016 (2021)
2. S. Ahmadi, N. Rabiee, Y. Fatahi, S.E. Hooshmand, M. Bagherzadeh, M. Rabiee, V. Jajarmi, R. Dinarvand, S. Habibzadeh, M.R. Saeb, R.S. Varma, M. Shokouhimehr, M.R. Hamblin, Sustain. Chem. Pharm. **21**, 100415 (2021)
3. M. Lu, P.D. Uchil, W. Li, D. Zheng, D.S. Terry, J. Gorman, W. Shi, B. Zhang, T. Zhou, S. Ding, R. Gasser, J. Prévost, G. Beaudoin-Bussières, S.P. Anand, A. Laumaea, J.R. Grover, L. Liu, D.D. Ho, J.R. Mascola, A. Finzi, P.D. Kwong, S.C. Blanchard, W. Mothes, Cell Host Microbe **28**, 880 (2020)
4. G. Singh, A. Saini, A. Kaur, J. Mol. Struct. **1250**, 131858 (2022)
5. S. Yalçın, S. Yalçınkaya, F. Ercan, J. Mol. Struct. **1240**, 130556 (2021)
6. L.A. Anthony, P. Nethaji, G. Sundararajan, D. Rajaraman, J. Mol. Struct. **1250**, 131892 (2022)
7. R.K. Hussein, H.M. Elkhair, J. Mol. Struct. **1231**, 129979 (2021)
8. S.A. Almalki, T.M. Bawazeer, B. Asghar, A. Alharbi, M.M. Aljohani, M.E. Khalifa, N. El-Metwaly, J. Mol. Struct. **1244**, 130961 (2021)
9. Faheem, B.K. Kumar, K.V.G.C. Sekhar, S. Kunjiappan, J. Jamalis, R. Balaña-Fouce, B.L. Tekwani, M. Sankaranarayanan, Bioorg. Chem. **104**, 104269 (2020)
10. M. Sathish, G. Meenakshi, S. Xavier, S. Sebastian, S. Periandy, N. Ahmad, J. Jamalis, M. Rosli, H.-K. Fun, J. Mol. Struct. **1164**, 420 (2018)
11. D. Matiadis, K.E. Nowak, E. Alexandratou, A. Hatzidimitriou, M. Sagnou, R. Papadakis, J. Mol. Liq. **331**, 115737 (2021)
12. M. Yusuf, P. Jain, Arab. J. Chem. **7**, 553 (2014)
13. I.M. El-Deen, A.F. Shoair, M.A. El-Bindary, J. Mol. Liq. **249**, 533 (2018)
14. M.M. Abdulla, A.E.-G.E. Amr, A.A. Hussain, M.A. Al-Omar, A.F.A. Shalaby, Res. Chem. Intermed. **41**, 127 (2015)
15. S.S. Korgaokar, P.H. Patel, M.J. Shah, H.H. Parekh, Indian J. Pharm. Sci. **58**, 222 (1996)
16. E.C. Taylor, H.H. Patel, Tetrahedron **48**, 8089 (1992)
17. D. Nauduri, G.B.S. Reddy, Chem. Pharm. Bull. **46**, 1254 (1998)
18. R.H. Udupi, A.S. Kushnoor, A.R. Bhat, Indian J. Heterocycl. Chem. **8**, 63 (1998)
19. Z. Özdemir, H.B. Kandilci, B. Gümüşel, U. Çaliş, A.A. Bilgin, Eur. J. Med. Chem. **42**, 373 (2007)
20. E. Palaska, M. Aytemir, I.T. Uzbay, D. Erol, Eur. J. Med. Chem. **36**, 539 (2001)
21. H. Deng, Z.Y. Yu, G.Y. Shi, M.J. Chen, K. Tao, T.P. Hou, Chem. Biol. Drug Des. **79**, 279 (2012)
22. M. Rani, M. Yusuf, S.A. Khan, P. Sahota, G. Pandove, Arab. J. Chem. **8**, 174 (2015)
23. P.V. Sowmya, B. Poojary, B.C. Revanasiddappa, M. Vijayakumar, P. Nikil, V. Kumar, Res. Chem. Intermed. **43**, 7399 (2017)
24. F. Puig-Basagoiti, M. Tilgner, B.M. Forshey, S.M. Philpott, N.G. Espina, D.E. Wentworth, S.J. Goebel, P.S. Masters, B. Falgout, P. Ren, D.M. Ferguson, P.Y. Shi, Antimicrob. Agents Chemother. **50**, 1320 (2006)
25. G. Singh, A. Goyal, R.S. Bhatti, S. Arora, Bionatura **4**, 994 (2019)
26. D. Havrylyuk, B. Zimenkovsky, O. Vasylenko, R. Lesyk, J. Heterocycl. Chem. **50**, E55 (2013)
27. S. Abu-Melha, M.M. Edrees, S.M. Riyadh, M.R. Abdelaziz, A.A. Elfiky, S.M. Gomha, Molecules **25**, 4565 (2020)

28. M.D. Hanwell, D.E. Curtis, D.C. Lonie, T. Vandermeersch, E. Zurek, G.R. Hutchison, J. Cheminform. **4**, 17 (2012)
29. G.M. Morris, D.S. Goodsell, R.S. Halliday, R. Huey, W.E. Hart, R.K. Belew, A.J. Olson, J. Comput. Chem. **19**, 1639 (1998)
30. A. Akdemir, A. Angeli, F. Göktaş, P. Eraslan Elma, N. Karalı, C.T. Supuran, J. Enzyme Inhib. Med. Chem. **34**, 528 (2019)
31. D. Biovia, H. Berman, J. Westbrook, Z. Feng, G. Gilliland, T. Bhat, H. Weissig, I. Shindyalov, P. Bourne, T. Darden, *Dassault systèmes BIOVIA, Discovery Studio Visualizer, v. 17.2*. (Dassault Systèmes, San Diego, 2016). J. Chem. Phys (2000) [cited 10; 21].
32. O. Trott, A.J. Olson, J. Comput. Chem. **31**, 455 (2010)
33. A.H. Hasan, N.H. Hussen, S. Shakya, J. Jamalis, M.R.F. Pratama, S. Chander, H. Kharkwal, S. Murugesan, Struct. Chem. **33**, 1645 (2022) https://doi.org/10.1007/s11224-022-01996-y
34. A.H. Hasan, S. Murugesan, S.I. Amran, S. Chander, M.M. Alanazi, T.B. Hadda, S. Shakya, M.R.F. Pratama, B. Das, S. Biswas, J. Jamalis, Bioorg. Chem. **119**, 105572 (2022)
35. G.W.T.M.J. Frisch, H.B. Schlegel, G.E. Scuseria, M.A. Robb, J.R. Cheeseman, G. Scalmani, V. Barone, G.A. Petersson, H. Nakatsuji, X. Li, M. Caricato, A. Marenich, J. Bloino, B.G. Janesko, R. Gomperts, B. Mennucci, H.P. Hratchian, J.V. Ortiz, A.F. Izmaylov, J.L. Sonnenberg, D. Williams-Young, F. Ding, F. Lipparini, F. Egidi, J. Goings, B. Peng, A. Petrone, T. Henderson, D. Ranasinghe, V.G. Zakrzewski, J. Gao, N. Rega, G. Zheng, W. Liang, M. Hada, M. Ehara, K. Toyota, R. Fukuda, J. Hasegawa, M. Ishida, T. Nakajima, Y. Honda, O. Kitao, H. Nakai, T. Vreven, K. Throssell, J.A. Montgomery Jr., J.E. Peralta, F. Ogliaro, M. Bearpark, J.J. Heyd, E. Brothers, K.N. Kudin, V.N. Staroverov, T. Keith, R. Kobayashi, J. Normand, K. Raghavachari, A. Rendell, J.C. Burant, S.S. Iyengar, J. Tomasi, M. Cossi, J.M. Millam, M. Klene, C. Adamo, R. Cammi, J.W. Ochterski, R.L. Martin, K. Morokuma, O. Farkas, J.B. Foresman, D.J. Fox, *Gaussian 16* (Gaussian Inc., Wallingford CT, 2009)
36. A.D. Becke, J. Chem. Phys. **98**, 5648 (1993)
37. P.C. Hariharan, J.A. Pople, Chem. Phys. Lett. **16**, 217 (1972)
38. A. Yildirim, F.A. Celik, M. Çıbuk, E. Yilmaz, Chem. Phys. Lett. **792**, 139390 (2022)
39. E. Tanış, J. Mol. Liq. **358**, 119161 (2022)
40. N. Çankaya, S.Y. Azarkan, E. Tanış, Drug Chem. Toxicol. 1 (2021) https://doi.org/10.1080/01480545.2021.1894711
41. S. Celik, E. Tanıs, Comput. Theor. Chem. **1212**, 113709 (2022)
42. E. Tanış, J. Electron. Mater. **51**, 4978 (2022)https://doi.org/10.1007/s11664-022-09730-4
43. G.A. Zhurko, D. Zhurko, Ivanovo, Russia, Academic version 1.5 (2004)
44. S. Mahmud, S. Biswas, G.K. Paul, M.A. Mita, M.M. Promi, S. Afrose, M.R. Hasan, S. Zaman, M.S. Uddin, K. Dhama, T.B. Emran, M.A. Saleh, J. Simal-Gandara, Biology **10**, 589 (2021)
45. S. Chander, P. Ashok, Y.-T. Zheng, P. Wang, K.S. Raja, A. Taneja, S. Murugesan, Bioorg. Chem. **64**, 66 (2016)
46. C.A. Lipinski, F. Lombardo, B.W. Dominy, P.J. Feeney, Adv. Drug Deliv. Rev. **46**, 3 (2001)
47. L.Z. Benet, C.M. Hosey, O. Ursu, T.I. Oprea, Adv. Drug Deliv. Rev. **101**, 89 (2016)
48. P. Banerjee, A.O. Eckert, A.K. Schrey, R. Preissner, Nucleic Acids Res. **46**, W257 (2018)
49. S. Shakya, I.M. Khan, M. Ahmad, J. Photochem. Photobiol. A **392**, 112402 (2020)
50. M.D. Khan, S. Shakya, H.H. Thi Vu, L. Habte, J.W. Ahn, J. Environ. Manag. **280**, 111652 (2021)
51. M.R. Islam, S. Shakya, A. Selim, M.S. Alam, M. Ali, J. Chem. Eng. Data **64**, 4169 (2019)
52. S. Murugavel, C. Ravikumar, G. Jaabil, P. Alagusundaram, J. Mol. Struct. **1176**, 729 (2019)
53. I.M. Khan, S. Shakya, ACS Omega **4**, 9983 (2019)